16th World Conference on Earthquake Engineering, 16WCEE 2017
Santiago Chile, January 9th to 13th 2017
Paper N° XXXX (1471)
Registration Code: S-XXXXXXXX

AN IMPROVED HYSTERESIS MODEL FOR CIRCULAR REINFORCED AND SQUARE REINFORCED CONCRETE COLUMNS UNDER CYCLIC TORSIONAL LOADING

T. Ghosh Mondal[(1)], S. R. Kothamuthyala[(2)], S. S. Prakash[(3)]

[(1)] *Graduate Student, Department of Civil Engineering, IIT Hyderabad, Email: ce13m1023@iith.ac.in*
[(2)] *Graduate Student, Department of Civil Engineering, IIT Hyderabad, Email: ce15mtech11023@iith.ac.in*
[(3)] *Faculty, Department of Civil Engineering, IIT Hyderabad, Email: suriyap@iith.ac.in*

Abstract

It has been observed in the past that, reinforced concrete (RC) bridge columns are, very often, subjected to torsional moment in addition to flexure and shear during seismic vibration. However, the torsional moment is generally ignored in typical design practices. Previous studies have shown that, ignoring torsional moment may lead to brittle shear failure of the columns triggering collapse of the entire or part of the bridge structure. Therefore, rational models need to be developed to consider the effect of torsion in the design of RC bridge columns. Performance based seismic design is an emerging design concept which calls for accurate prediction of the hysteresis behavior of structural elements to ensure safe and sustainable design under earthquake loading. However, very few investigations in the past focused on the development of analytical model to accurately predict the response of RC members under cyclic torsion. Though quite a good number of models are available for prediction of shear and flexural hysteresis, they are not readily applicable for torsion owing to significant pinching and stiffness degradation associated with torsional loading. Hysteresis models taking into account pinching and stiffness degradation effect under cyclic torsional loading are scarce. The present study aims at filling this knowledge gap by proposing an improved polygonal hysteresis model which can accurately predict the hysteretic behavior of RC circular and square columns under torsion. The proposed empirical model is validated through experimental data of two circular columns and two square columns tested under pure torsion. Close correlation is observed between the predicted and measured torque-twist curves.

Keywords: Polygonal hysteresis model; RC column; torsion; primary curve; unloading and reloading rules.

1. Introduction

Reinforced concrete bridge columns are subjected to torsional loading under various conditions [1]. Torsion in columns can be induced by skewed or horizontally curved bridges, bridges with unequal spans or column heights, and bridges with outrigger bents. Torsional moment needs special attention in design as it may otherwise trigger brittle shear dominated failure of members. Collapse of many important bridges around the world caused by recent earthquakes has put forth the necessity to assess the seismic vulnerability of the existing bridge columns under torsion. Seismic analysis of reinforced concrete (RC) structures requires hysteresis models that can accurately predict strength, stiffness, and ductility characteristics of the members under cyclic loading. Bridge columns should be properly designed to adequately dissipate seismic energy through inelastic deformation under vibrations during earthquakes [2-3]. The level of accuracy of seismic design depends on the accuracy of the hysteresis model. Owing to all these reasons, it is of utmost importance to have a proper hysteresis model which can accurately predict the cyclic flexural behavior of RC members considering strength and stiffness degradation along with the pinching effects.

Polygonal hysteresis models are a well-established modeling approach, where the response of a member to cyclic loading is governed by a set of control points and paths defined by piecewise linear or nonlinear functions. One of the best known polygonal hysteresis models available in literature is Clough and Johnston (1966) [4] model, which is characterized by a bilinear primary curve. It considers strain hardening in post yielding regime and takes into account stiffness degradation under load reversals. Takeda model [5] represents a tri-linear primary curve marked by a stiffness change at cracking point. It is governed by some loading – unloading rules formulated based on experimental observations. In the pivot hysteresis model developed by Dowell et al. (1998) [6], the envelope curve under monotonic loading has four branches characterized by elastic stiffness, strain hardening, strength degradation and linearly decreasing residual strength. The loading and unloading are governed by two pivot points which determine the level of softening with increasing displacement and the degree of pinching on load reversal. Other notable works on PHM include Fukada (1969) [7], Aoyama (1971) [8], Atalay and Penzien (1975) [9], Nakata et al. (1978) [10], and Mansur and Hsu (2005) [11]. However, all these models were developed for shear and flexure and are incapable of predicting the behavior under torsion [12] owing to high degree of pinching and degradation involved in torsional loading. Very few researchers have, indeed, focused on the analytical modeling of the hysteresis behavior exhibited by RC members under cyclic torsion. Tirasit and Kawashima (2007) [13] and Wang et al. (2014) [12] have recently proposed some PHMs for RC columns under torsional loading. In both of the studies, a semi-empirical primary curve was used, where the yield torsional moment was estimated using space truss analogy [14, 15] and post-yield behavior was obtained from empirical relations derived on the basis of experimental observations. In this study, an entirely mechanics based primary curve is proposed using SMMT (softened membrane model for torsion) [16] which is more reliable than the empirical equations based approach. Moreover, the previous studies did not consider any slope change in the primary curve at the cracking point, in contrast to the actual behavior observed during experiments. The present study tends to eliminate this discrepancy by introducing a slope change at the cracking point. Loading - unloading rules are proposed based on statistical analysis of experimental data which are at variance with the previous models. An additional control point has been introduced in the unloading branch to better predict the actual behavior. It was observed that the proposed model closely predicts the measured load – displacement behavior.

2. Experimental Program

The specimens used for formulation and validation of the proposed model were tested at University of Missouri [17] under pure cyclic torsion. The geometric configuration and reinforcement content of the specimens are summarized in Table 1. The cross sectional details are shown in Fig. 1. Cyclic torsional loading was generated by controlling two horizontal servo-controlled hydraulic actuators. The axial compressive load was applied by a hydraulic jack on top of the load stubs as shown in Fig. 2.

Table 1 - Specimen Details

Specimen Id/ Parameters	H/D(3)-T/M((∞)-1.32%	H/D(6)-T/M(∞)-0.73%
Section Shape	Circular	Circular
Diameter/Width (mm)	610	610
Clear Cover (mm)	25	25
Total Column Height (m)	2.74	4.55
Effective Column Height (m)	1.83	3.65
Cylinder Strength of Concrete (MPa)	27.97	37.90
Longitudinal Steel Yield Strength (MPa)	462	462
Transverse Steel Yield Strength (MPa)	457	457
Transverse Steel Ratio (percentage)	1.32	0.73
Longitudinal Steel Ratio (percentage)	2.1	2.1
Axial Force (kN)	600.51	600.51

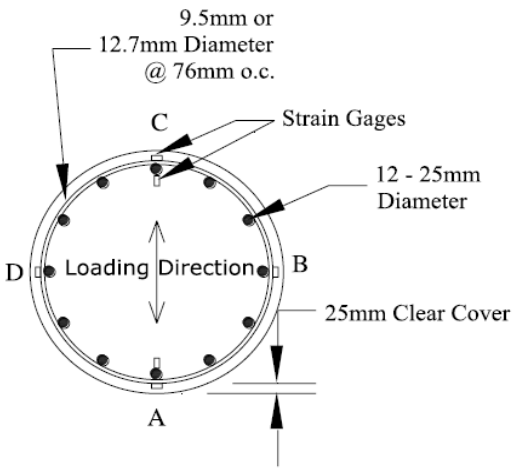

Fig. 1 - Specimen Cross Section [17]

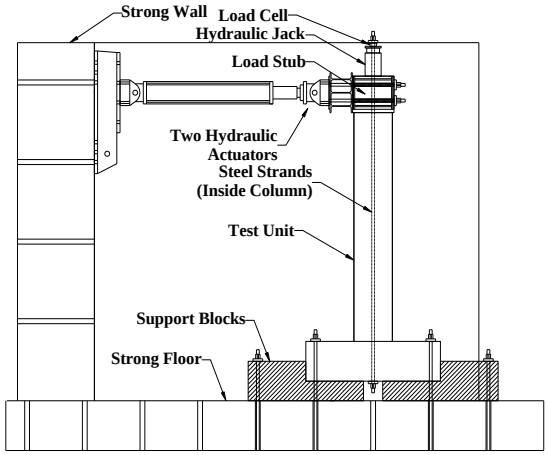

Fig. 2 - Test Set-up [17]

3. Hysteresis Model Description

Any PHM is governed by primary (backbone) curve (Fig. 3 and 4) and loading/unloading rules (Fig. 5). A number of control points (Figs. 5(b) and 5(d)) are fixed which regulate the hysteresis loops. Paths joining successive control points are called branches ((Figs. 5(a) and 5(c))). Transition from one control point to another is governed by a set of rules which are determined empirically from experimental data (Figs. 6-12). The details of the model are described below.

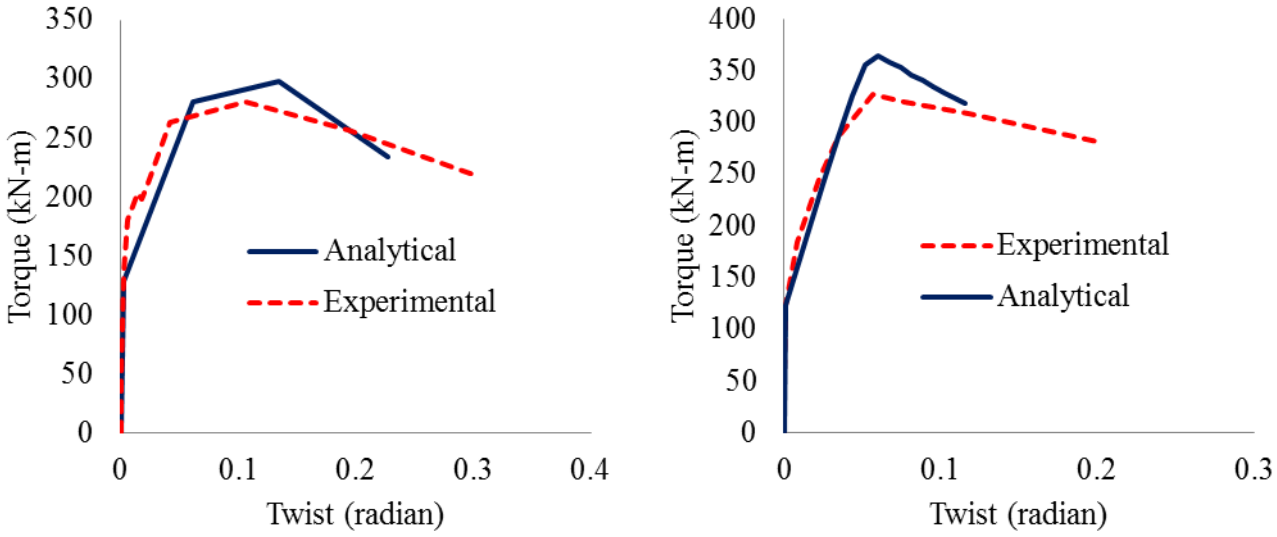

(a) H/D(6)-T/M(∞)-0.73% (b) H/D(3)-T/M(∞)-1.32%

Fig. 3 - Primary Curve under Torsion [18]

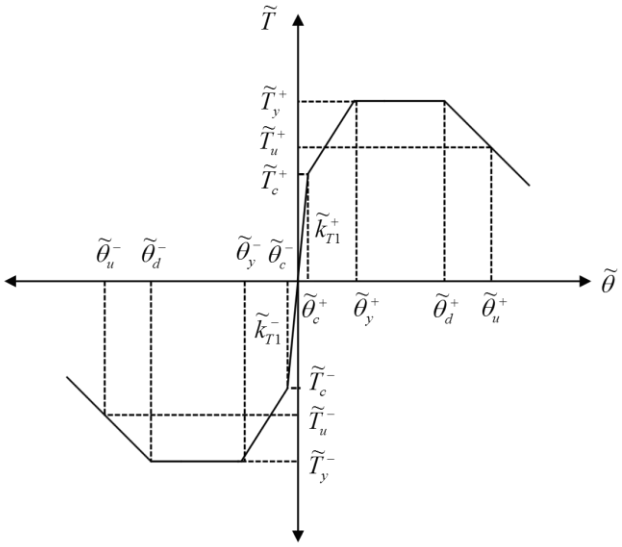

Fig. 4 - Idealized Primary Curve

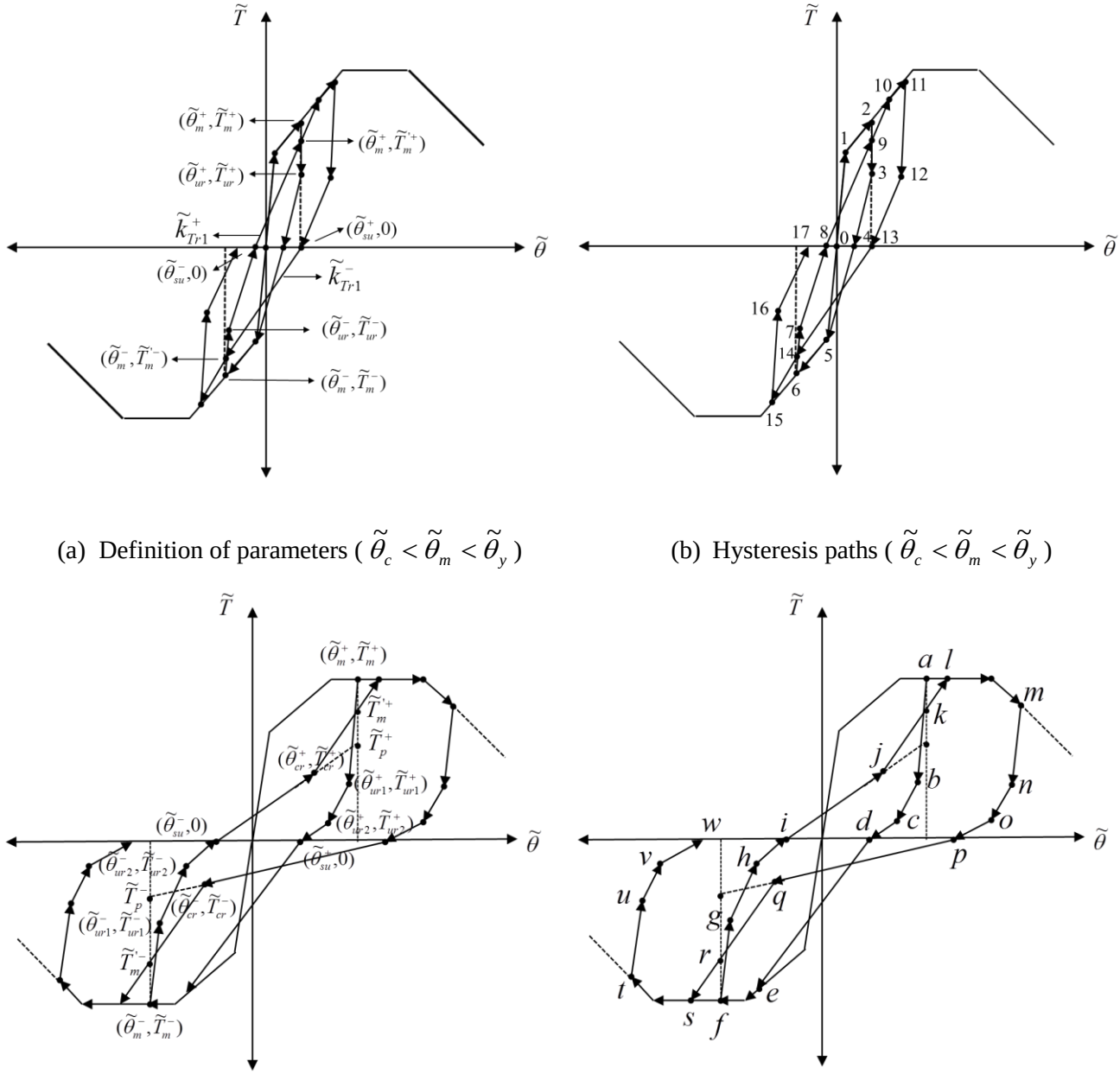

(a) Definition of parameters ($\widetilde{\theta}_c < \widetilde{\theta}_m < \widetilde{\theta}_y$)

(b) Hysteresis paths ($\widetilde{\theta}_c < \widetilde{\theta}_m < \widetilde{\theta}_y$)

(c) Definition of parameters ($\widetilde{\theta}_m > \widetilde{\theta}_y$)

(d) Hysteresis paths ($\widetilde{\theta}_m > \widetilde{\theta}_y$)

Fig. 5 Characteristics of hysteresis loops

3.1. Primary Curve

Primary curve is the envelope of the cyclic torque– twist behavior. It is assumed to be identical to the behavior under monotonic loading. In previous studies [12, 13], the primary curve was estimated using a semi-empirical model, where the yield torsional moment was calculated using space truss analogy. However, in the present study, a more rational analytical model, known as SMMT (Softened Membrane Model for Torsion), was used to obtain the backbone curve. The details of SMMT are nicely explained in Ganganagoudar et al. 2016 [18]. The authors used the same specimens as used in this study to show that SMMT can accurately predict backbone curve under cyclic torsion. Therefore, the backbone curves (Fig. 3) are directly adopted from the aforementioned

study without any alteration. A change in slope in primary curve at the cracking point has been introduced in this model which was ignored by the previous researchers [12, 13]. The primary curve obtained from SMMT is idealized as piecewise linear functions representing elastic stiffness, strain hardening, yield plateau, and strength deterioration as shown in Fig. 4.

3.2. Unloading Rules

1. The unloading path follows the initial stiffness of the primary curve (path $1 \rightarrow 0$, $5 \rightarrow 0$) if torsion at the beginning of the unloading is less than the cracking torsion ($\tilde{T}_m \le \tilde{T}_c$), and $\tilde{T}_c$ has not been previously exceeded in either direction.
2. After cracking, the unloading path becomes a function of internal variables such as displacement (rotational) ductility ($\tilde{\theta}_m/\tilde{\theta}_c$ for $\tilde{\theta}_c < \tilde{\theta}_m < \tilde{\theta}_y$, $\tilde{\theta}_m/\tilde{\theta}_y$ for $\tilde{\theta}_m > \tilde{\theta}_y$) and current deformation level. From a given unloading point on the primary curve ($\tilde{\theta}_m, \tilde{T}_m$), the hysteresis path is directed towards ($\tilde{\theta}_{ur1}, \tilde{T}_{ur1}$) (path $2 \rightarrow 3$, $6 \rightarrow 7$, $11 \rightarrow 12$, $15 \rightarrow 16$, $a \rightarrow b$, $f \rightarrow g$, $m \rightarrow n$, $t \rightarrow u$) which is estimated using the expressions shown in Eq. 1 (Figs. 6 and 7).

   i. For Circular Columns:

$$\tilde{\theta}_{ur1}/\tilde{\theta}_m = -0.0028\left(\tilde{\theta}_m/\tilde{\theta}_c\right) + 1.0498 \quad \text{for } \tilde{\theta}_c < \tilde{\theta}_m < \tilde{\theta}_y \tag{1a}$$

$$= -0.0004\left(\tilde{\theta}_m/\tilde{\theta}_y\right) + 1.0047 \quad \text{for } \tilde{\theta}_m > \tilde{\theta}_y \tag{1b}$$

$$\tilde{T}_{ur1}/\tilde{T}_m = -0.0009\left(\tilde{\theta}_m/\tilde{\theta}_c\right) + 0.8527 \quad \text{for } \tilde{\theta}_c < \tilde{\theta}_m < \tilde{\theta}_y \tag{1c}$$

$$= -0.0006\left(\tilde{\theta}_m/\tilde{\theta}_y\right) + 0.8623 \quad \text{for } \tilde{\theta}_m > \tilde{\theta}_y \tag{1d}$$

   ii. For Square Columns

$$\frac{\tilde{\theta}_{ur1}}{\tilde{\theta}_m} = -0.026\left(\frac{\tilde{\theta}_m}{\tilde{\theta}_c}\right) + 0.904 \quad \text{for } \tilde{\theta}_c < \tilde{\theta}_m < \tilde{\theta}_y \tag{1e}$$

$$= 0.008\left(\frac{\tilde{\theta}_m}{\tilde{\theta}_y}\right) + 0.931 \quad \text{for } \tilde{\theta}_m > \tilde{\theta}_y \tag{1f}$$

$$\frac{\tilde{T}_{ur1}}{\tilde{T}_m} = -0.049\left(\frac{\tilde{\theta}_m}{\tilde{\theta}_c}\right) + 0.783 \quad \text{for } \tilde{\theta}_c < \tilde{\theta}_m < \tilde{\theta}_y \tag{1g}$$

$$= -0.065\left(\frac{\tilde{\theta}_m}{\tilde{\theta}_y}\right) + 0.846 \quad \text{for } \tilde{\theta}_m > \tilde{\theta}_y \tag{1h}$$

3. In case of unloading beyond the yield point ($\tilde{\theta}_m > \tilde{\theta}_y$), from ($\tilde{\theta}_{ur1}, \tilde{T}_{ur1}$), the unloading path leads to ($\tilde{\theta}_{ur2}, \tilde{T}_{ur2}$) (path $b \rightarrow c$, $g \rightarrow h$, $n \rightarrow o$, $u \rightarrow v$), which is given by Eq. 2 (Fig. 8).

   i. For Circular Columns:

$$\frac{\tilde{\theta}_{ur2}}{\tilde{\theta}_m} = 0.0363\left(\frac{\tilde{\theta}_m}{\tilde{\theta}_y}\right) + 0.7101 \tag{2a}$$

$$\frac{\tilde{T}_{ur2}}{\tilde{T}_m} = -0.0126\left(\frac{\tilde{\theta}_m}{\tilde{\theta}_y}\right) + 0.3243 \quad (2b)$$

ii. For Square Columns:

$$\frac{\tilde{\theta}_{ur2}}{\tilde{\theta}_m} = 0.083\left(\frac{\tilde{\theta}_m}{\tilde{\theta}_y}\right) + 0.506 \quad (2c)$$

$$\frac{\tilde{T}_{ur2}}{\tilde{T}_m} = -0.057\left(\frac{\tilde{\theta}_m}{\tilde{\theta}_y}\right) + 0.312 \quad (2d)$$

4. Next, the hysteresis loop proceeds straight towards $(\tilde{\theta}_{su},0)$ on the zero load axis (path $3\rightarrow4$, $7\rightarrow8$, $12\rightarrow13$, $16\rightarrow17$, $c\rightarrow d$, $h\rightarrow i$, $o\rightarrow p$, $v\rightarrow w$). The reloading point $(\tilde{\theta}_{su},0)$ can be calculated as shown in Eq. 3 (Fig. 9).

i. For Circular Columns:

$$\tilde{\theta}_{su}/\tilde{\theta}_m = -0.0015\left(\tilde{\theta}_m/\tilde{\theta}_c\right) + 0.2358 \quad \text{for } \tilde{\theta}_c < \tilde{\theta}_m < \tilde{\theta}_y \quad (3a)$$

$$= 0.1012\left(\tilde{\theta}_m/\tilde{\theta}_y\right) + 0.0848 \quad \text{for } \tilde{\theta}_m > \tilde{\theta}_y \quad (3b)$$

ii. For Square Columns:

$$\frac{\tilde{\theta}_{su}}{\tilde{\theta}_m} = 0.015\left(\frac{\tilde{\theta}_m}{\tilde{\theta}_c}\right) + 0.19 \quad \text{for } \tilde{\theta}_c < \tilde{\theta}_m < \tilde{\theta}_y \quad (3c)$$

$$= 0.151\left(\frac{\tilde{\theta}_m}{\tilde{\theta}_y}\right) + 0.14 \quad \text{for } \tilde{\theta}_m > \tilde{\theta}_y \quad (3d)$$

i. For Circular Columns:

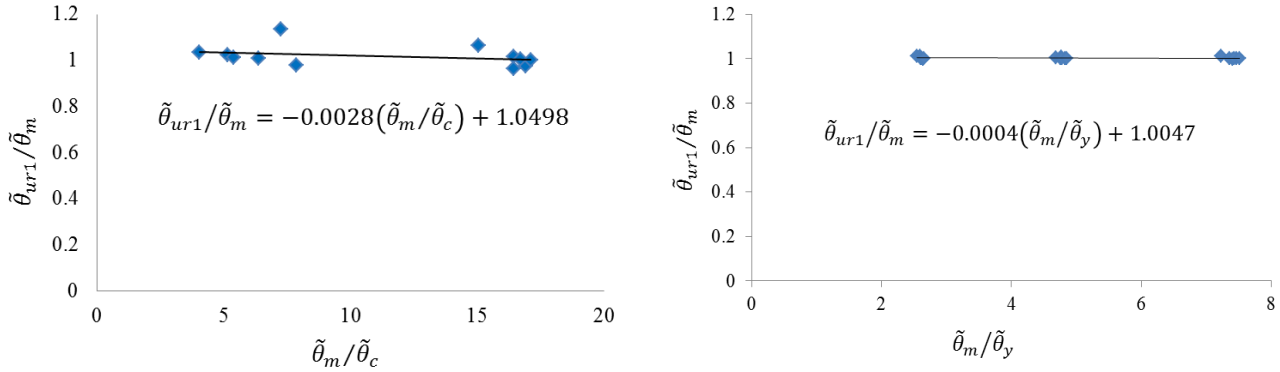

(a) $\tilde{\theta}_c < \tilde{\theta}_m < \tilde{\theta}_y$ (b) $\tilde{\theta}_m > \tilde{\theta}_y$

Fig. 6 - Dependence of $\tilde{\theta}_{ur1}/\tilde{\theta}_m$ on ductility ratio for circular columns

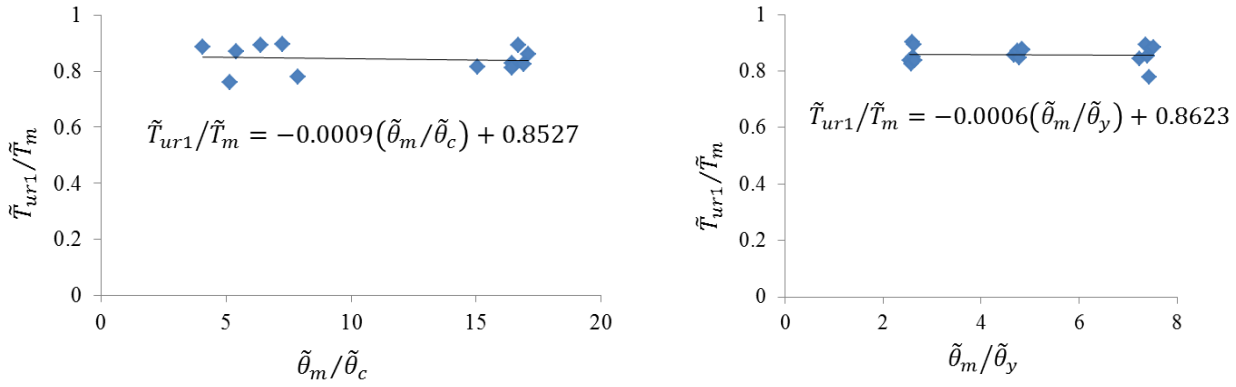

(a) $\tilde{\theta}_c < \tilde{\theta}_m < \tilde{\theta}_y$ (b) $\tilde{\theta}_m > \tilde{\theta}_y$

Fig. 7 - Dependence of $\tilde{T}_{ur1}/\tilde{T}_m$ on ductility ratio for circular columns

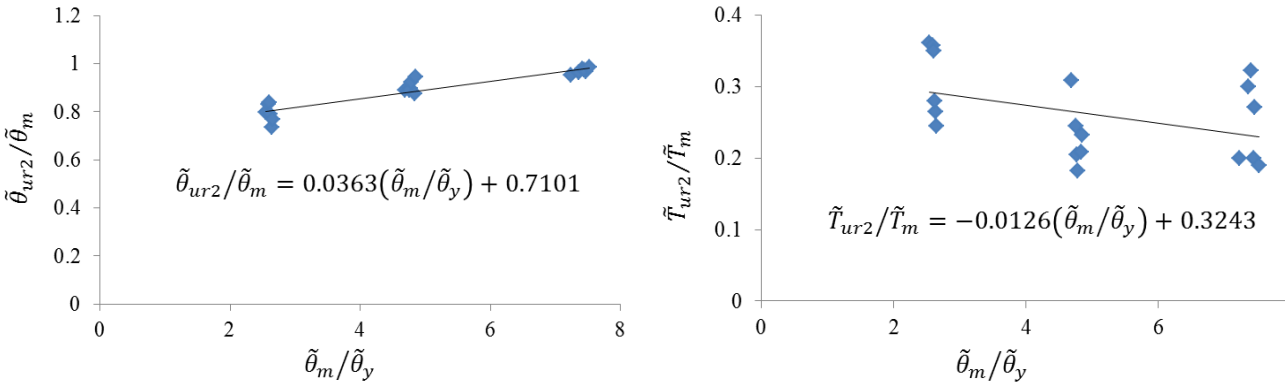

Fig. 8 - Dependence of $\tilde{\theta}_{ur2}/\tilde{\theta}_m$ and $\tilde{T}_{ur2}/\tilde{T}_m$ on $\tilde{\theta}_m/\tilde{\theta}_y$ for circular columns

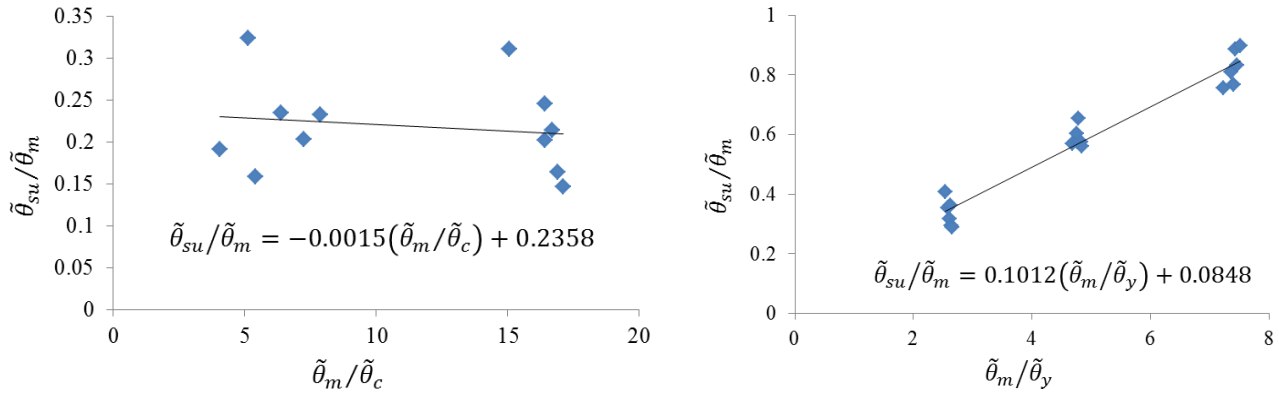

(a) $\tilde{\theta}_c < \tilde{\theta}_m < \tilde{\theta}_y$ (b) $\tilde{\theta}_m > \tilde{\theta}_y$

Fig. 9 - Dependence of $\tilde{\theta}_{su}/\tilde{\theta}_m$ on ductility ratio for circular columns

ii. For Square Columns:

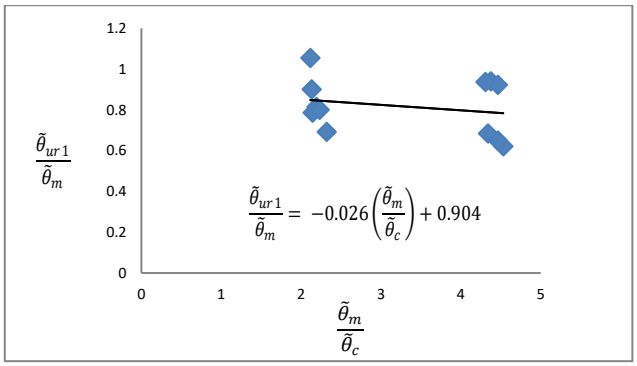

(c) $\tilde{\theta}_c < \tilde{\theta}_m < \tilde{\theta}_y$

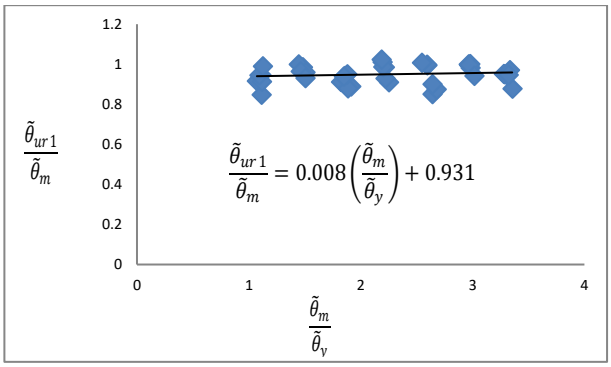

(d) $\tilde{\theta}_m > \tilde{\theta}_y$

Fig. 10 - Dependence of $\tilde{\theta}_{ur1}/\tilde{\theta}_m$ on ductility ratio for Square columns

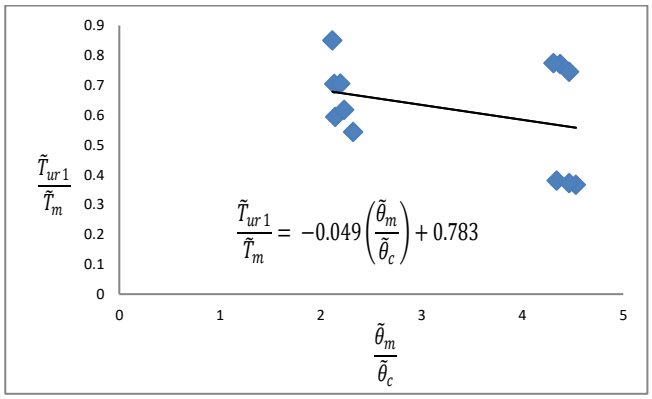

(c) $\tilde{\theta}_c < \tilde{\theta}_m < \tilde{\theta}_y$

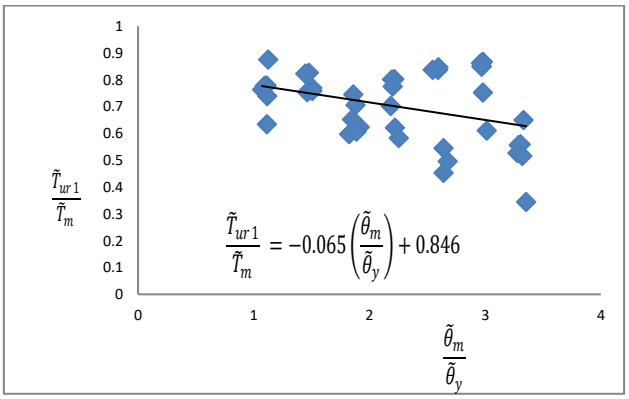

(d) $\tilde{\theta}_m > \tilde{\theta}_y$

Fig. 11 - Dependence of $\tilde{T}_{ur1}/\tilde{T}_m$ on ductility ratio for Square columns

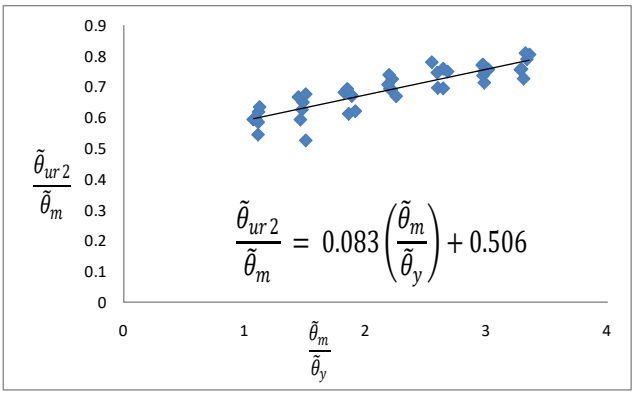

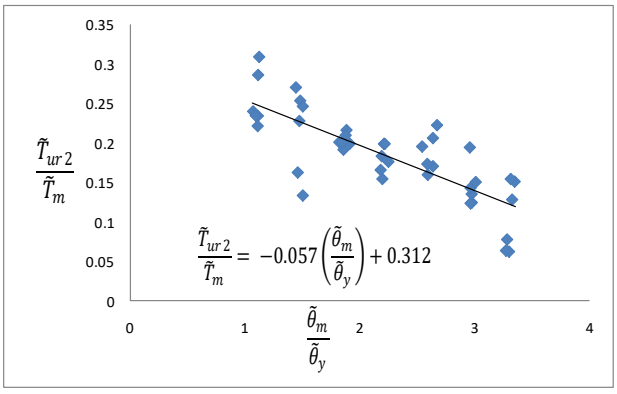

Fig. 12 - Dependence of $\tilde{\theta}_{ur2}/\tilde{\theta}_m$ and $\tilde{T}_{ur2}/\tilde{T}_m$ on $\tilde{\theta}_m/\tilde{\theta}_y$ for Square columns

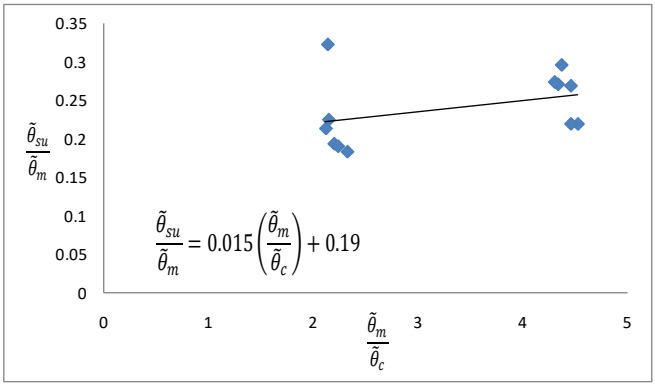

(c) $\tilde{\theta}_c < \tilde{\theta}_m < \tilde{\theta}_y$

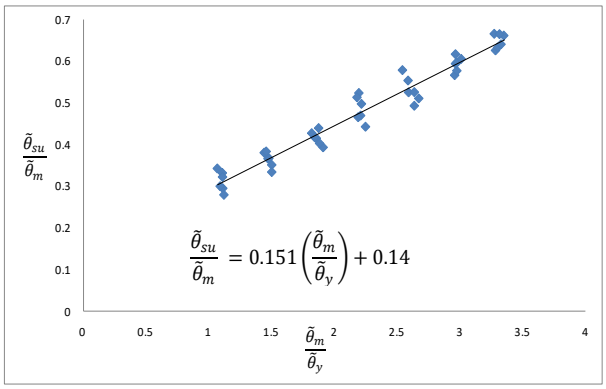

(d) $\tilde{\theta}_m > \tilde{\theta}_y$

Fig. 13 - Dependence of $\tilde{\theta}_{su}/\tilde{\theta}_m$ on ductility ratio for Square columns

3.3. Loading/reloading Rules

1. Initial loading and reloading follow the primary curve (path $1 \rightarrow 0$, $5 \rightarrow 0$) until the load is reversed at a level higher than the cracking load.
2. After cracking, the first loading in the opposite direction is directed towards the cracking load in the opposite direction (path $4 \rightarrow 5$).
3. When cracking load on both directions has been reached, the reloading path, till yielding, follows a straight line (path $8 \rightarrow 9$, $13 \rightarrow 14$) having a slope given by Eq. 4 (Fig. 10).

   i. For Circular Columns:

$$\tilde{k}_{Tr1}/\tilde{k}_{T1} = 0.7513\left(\tilde{\theta}_m/\tilde{\theta}_c\right)^{-0.786} \tag{4a}$$

   ii. For Square Columns:

$$\frac{\tilde{K}_{Tr1}}{\tilde{K}_{T1}} = -0.074\left(\frac{\tilde{\theta}_m}{\tilde{\theta}_c}\right) + 0.527 \tag{4b}$$

4. After yielding, reloading path up to $\tilde{\theta}_{cr}$ ($i \rightarrow j$, $p \rightarrow q$) follows a straight line passing through ($\tilde{\theta}_m, \tilde{T}_p$), which is estimated using Eq. 5 (Fig. 11).

   i. For Circular Columns:

$$\tilde{\theta}_{cr}/\tilde{\theta}_m = (-0.0067n + 0.0766)(\tilde{\theta}_m/\tilde{\theta}_y) + (0.0782n + 0.0037) \tag{5a}$$

$$\tilde{T}_p/\tilde{T}_m = (-0.0783n + 0.9425)(\tilde{\theta}_m/\tilde{\theta}_y)^{(0.1155n - 1.3943)} \leq 1 \tag{5b}$$

ii. For Square Columns:

$$\frac{\tilde{\theta}_{cr}}{\tilde{\theta}_m} = (-0.023n - 0.144)\left(\frac{\tilde{\theta}_m}{\tilde{\theta}_y}\right) + (0.086n - 0.018) \tag{5c}$$

$$\frac{\tilde{T}_p}{\tilde{T}_m} = (-0.034n - 0.214)\left(\frac{\tilde{\theta}_m}{\tilde{\theta}_y}\right) + (0.111n + 0.797) \tag{5d}$$

where, n is counter indicating number of cycles repeated at unloading point $\tilde{\theta}_m$. n is assigned a value of 1 when first unloading takes place at a given deformation level ($\tilde{\theta}_m$) and incremented every time load is reversed from any deformation level falling within the range of $(1 \pm 0.05)\tilde{\theta}_m$. n is computed separately for each direction of loading.

5. After ($\tilde{\theta}_{cr}, \tilde{T}_{cr}$), the loading path heads towards ($\tilde{\theta}_m, \tilde{T}'_m$) (path $j \to k$, $q \to r$). Calculation of $\tilde{T}'_m$ is governed by Eq. 6 (Fig. 12).

   i. For Circular Columns:

$$\tilde{T}'_m / \tilde{T}_m = -0.05557(\tilde{\theta}_m / \tilde{\theta}_y) + (0.0177n + 0.9842) \tag{6a}$$

   ii. For Square Columns:

$$\frac{\tilde{T}'_m}{\tilde{T}_m} = (-0.073n - 0.014)\left(\frac{\tilde{\theta}_m}{\tilde{\theta}_y}\right) + (0.385n + 0.507) \tag{6b}$$

6. Beyond the intersection of reloading branch with primary curve, the loading path follow the primary curve (path $l \to m$, $s \to t$).

i. For Circular Columns:

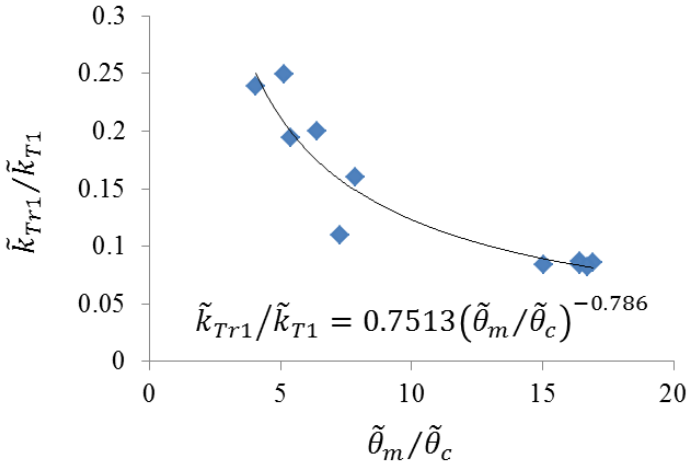

Fig. 14 - Dependence of $\tilde{k}_{Tr1}/\tilde{k}_{T1}$ on $\tilde{\theta}_m/\tilde{\theta}_c$

$\tilde{\theta}_{cr}/\tilde{\theta}_m = (-0.0067n + 0.0766)(\tilde{\theta}_m/\tilde{\theta}_y) + (0.0782n + 0.0037)$

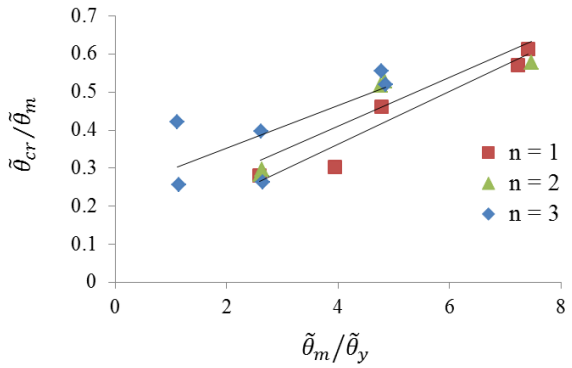

$\tilde{T}_p/\tilde{T}_m = (-0.0783n + 0.9425)(\tilde{\theta}_m/\tilde{\theta}_y)^{(0.1155n-1.3943)}$

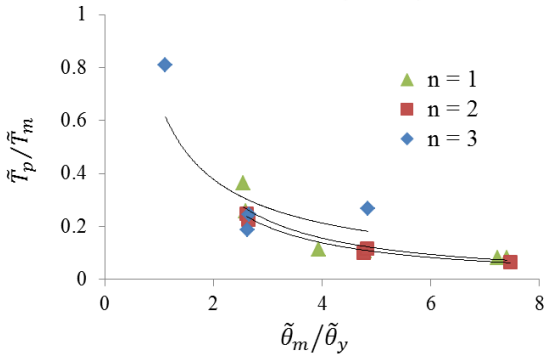

Fig. 15 - Dependence of $\tilde{\theta}_{cr}/\tilde{\theta}_m$ and $\tilde{T}_p/\tilde{T}_m$ on $\tilde{\theta}_m/\tilde{\theta}_y$

$\tilde{T'}_m/\tilde{T}_m = -0.05557(\tilde{\theta}_m/\tilde{\theta}_y) + (0.0177n + 0.9842)$

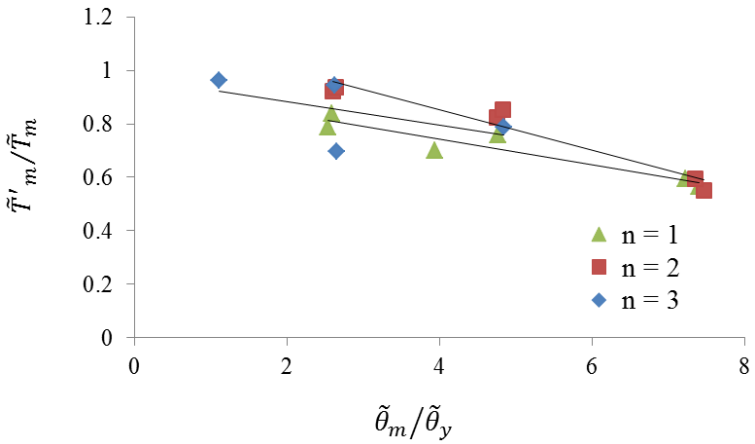

Fig. 16 - Dependence of $\tilde{T}'_m/\tilde{T}_m$ on $\tilde{\theta}_m/\tilde{\theta}_y$

ii. For Square Columns:

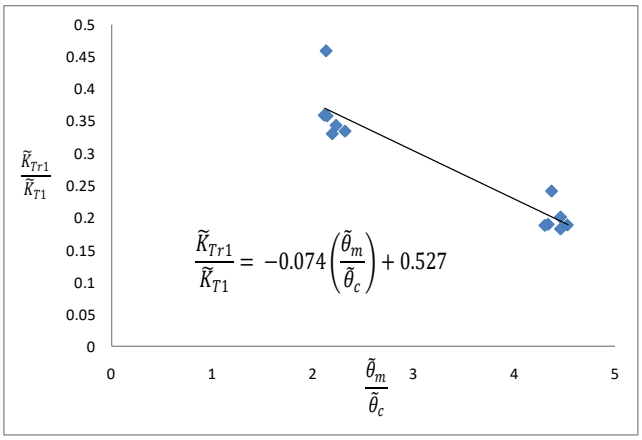

Fig. 17 - Dependence of $\tilde{k}_{Tr1}/\tilde{k}_{T1}$ on $\tilde{\theta}_m/\tilde{\theta}_c$

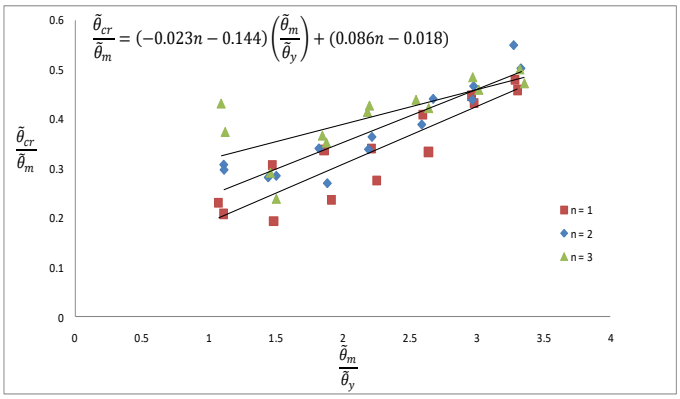

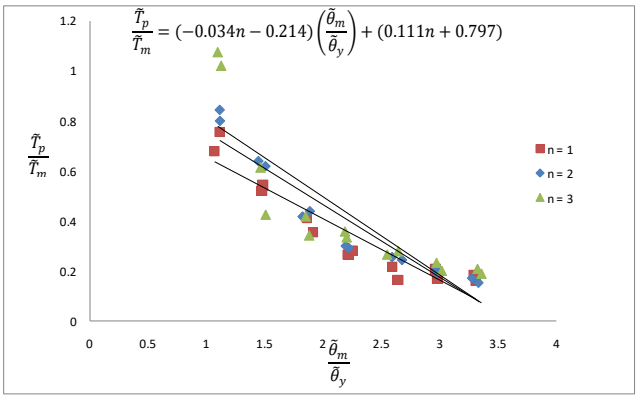

Fig. 18 - Dependence of $\tilde{\theta}_{cr}/\tilde{\theta}_m$ and $\tilde{T}_p/\tilde{T}_m$ on $\tilde{\theta}_m/\tilde{\theta}_y$

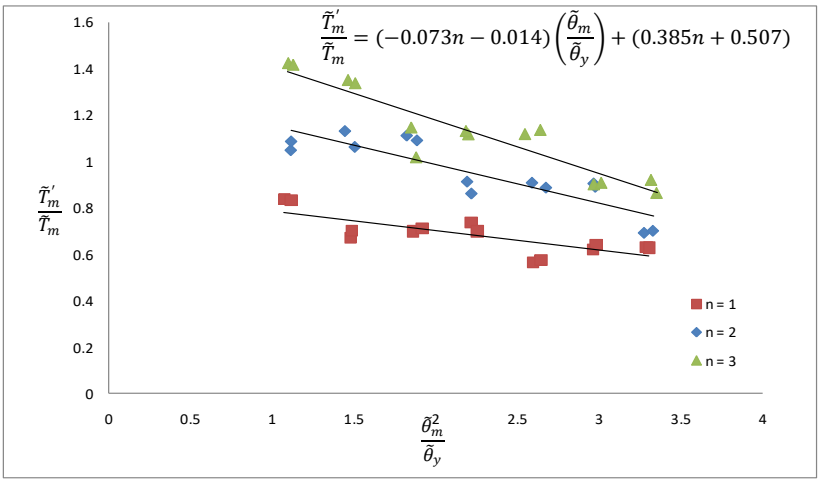

Fig. 19 - Dependence of $\tilde{T}'_m/\tilde{T}_m$ on $\tilde{\theta}_m/\tilde{\theta}_y$

4. Results and Discussion

4.1. Predictions of Torque-Twist Behavior

The torque-twist behavior predicted by the analytical model are presented and compared with experimental data in Fig. 13. It is observed that, the model predicted the experimental response of the columns reasonably well. It can also be seen from the graphs that the model was able to capture complex phenomena like strength and stiffness degradation along with pinching with appreciable accuracy.

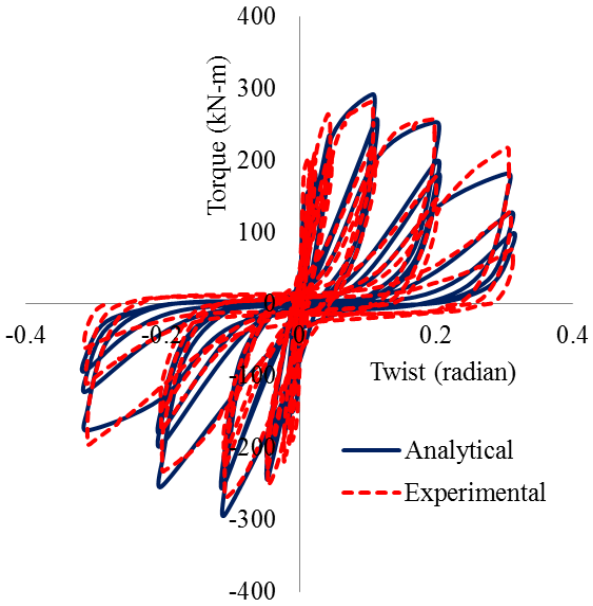

(a) H/D(6)-T/M(∞)-0.73%

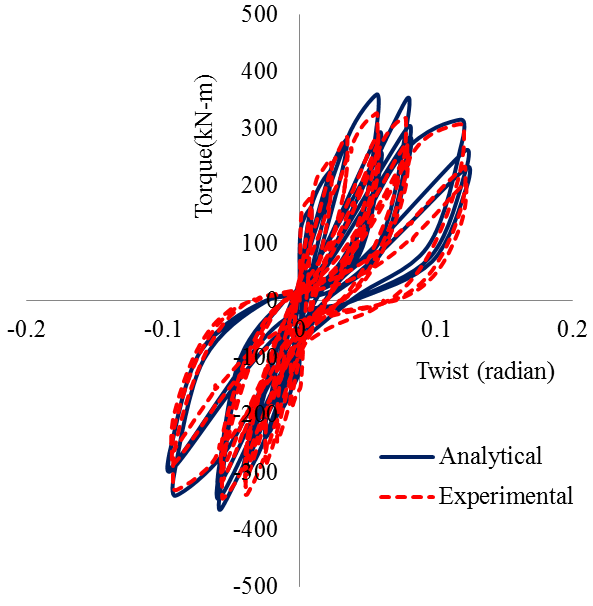

(b) H/D(3)-T/M(∞)-1.32%

Fig. 20 Prediction of Torsional Hysteresis

5. Conclusions

An improved PHM is proposed in this study for reinforced concrete circular columns subjected to torsion. Unloading and reloading rules are derived based on experimental observations. Primary curve is proposed to be estimated from SMMT. A slope change has been suggested at the cracking point unlike in the previous models. An additional point is also introduced in the unloading branch for more accurate prediction of the hysteresis loops. The analytical torque – twist behavior showed close correlation with experimental data. The proposed model can be extended in future to predict the hysteretic response of bridge columns under combined loading including torsion. Future studies could also focus on computer implementation of this hysteresis model to realize its utility fully on seismic analysis of bridge systems under torsional loading.

6. Acknowledgements

This analytical work is carried out as part of the project funded by SERB, Department of Science and Technology, India. Grant No. SB/S3/CEE/0060/2013. Their financial support is gratefully acknowledged.

7. References

[1] Mondal TG, Prakash SS (2015): Nonlinear Finite Element Analysis of RC Bridge Columns under Torsion with and without Axial Compression. *Journal of Bridge Engineering*, **21**(2), 04015037.

[2] Prakash SS, Belarbi A (2010): Towards damage-based design approach for RC bridge columns under combined loadings using damage index models. *Journal of Earthquake Engineering*, Taylor & Francis Group Journals, Vol. **14**, No. 3, pp. 363 – 389.

[3] Goodnight J, Kowalsky M, Nau J (2013): Effect of Load History on Performance Limit States of Circular Bridge Columns. *Journal of Bridge Engineering*, 10.1061/ (ASCE) BE.1943-5592.0000495, 1383-1396.

[4] Clough RW, Johnston SB (1966): Effects of Stiffness Degradation on Earthquake Ductility Requirements. *Proc. of the 2nd Japan Earthquake Engineering Symposium*, pp. 227—232.

[5] Takeda T, Sozen MA, Nielsen NN (1970): Reinforced Concrete Response to Simulated Earthquakes. *Journal of the Structural Division, ASCE*, Vo1. **96**, No. ST12, pp. 2557-2573.

[6] Dowell RK, Seible F, Wilson EL (1998): Pivot Hysteresis Model for Reinforced Concrete Members. *ACI Structural Journal*, Vol. **95** (5), pp. 607-617.

[7] Fukada Y (1969): A Study on the Restoring Force Characteristics of Reinforced Concrete Buildings. *Proc. of Kanto District Symposium*, Arch. Inst. of Japan, Tokyo, Japan, No. 40, (in Japanese).

[8] Aoyama H (1971): Analysis on a School Building Damaged During the Tockachi - Oki Earthquake. *Proc. of Kanto District Symposium*, Arch. Inst. of Japan, Tokyo, Jan.

[9] Atalay MB, Penzien J (1975): The Seismic Behavior of Critical Regions of Reinforced Concrete Components Influenced By Moment, Shear and Axial Force. *Report No. UCB/EERC/75/19*, University of California, Berkeley.

[10] Nakata S, Sproul T, Penzien J (1978): Mathematical Modeling of Hysteresis Loops for Reinforced Concrete Columns. *Report No. UCB/EERC/78/11*, University of California, Berkeley, California.

[11] Mansour M, Hsu T (2005): Behavior of Reinforced Concrete Elements under Cyclic Shear. I: Experiments. *Journal of Structural Engineering*, 10.1061/(ASCE)0733-9445(2005)131:1(44), 44-53.

[12] Wang P, Han Q, Du X (2014). Seismic performance of circular RC bridge columns with flexure–torsion interaction. *Soil Dynamics and Earthquake Engineering*, **66**, pp.13-30.

[13] Tirasit P, Kawashima K (2007): Seismic performance of square reinforced concrete columns under combined cyclic flexural and torsional loadings. *Journal of Earthquake Engineering*, **11**, 425-452.

[14] Rahal KL, Collins MP (1995): Analysis of sections subjected to combined shear and torsion-a theoretical model. *ACI Structural Journal*, **92**, 459-459.

[15] Mo YL, Yang RY (1996): Response of reinforced/prestressed concrete box structures to dynamically applied torsion. *Nuclear engineering and design*, **165**(1), 25-41.

[16] Hsu TT (1992): *Unified theory of reinforced concrete (Vol. 5)*. CRC press.

[17] Prakash, SS. (2009): Seismic behavior of circular reinforced concrete bridge columns under combined loading including torsion. *PhD Doctoral Dissertation*, University of Missouri Rolla.

[18] Ganganagoudar A, Mondal TG, Prakash SS (2016): Improved Softened Membrane Model for Reinforced Concrete Circular Bridge Columns under Torsional Loading. *Journal of Bridge Engineering*, p.04016037.